Energy & Environmental Science

Highly Efficient Transverse Thermoelectric Devices with Re_4Si_7 Crystals

Journal:	*Energy & Environmental Science*
Manuscript ID	EE-ART-03-2021-000923
Article Type:	Paper
Date Submitted by the Author:	26-Mar-2021

Complete List of Authors:	Scudder, Michael; The Ohio State University, Chemistry and Biochemistry He, Bin; The Ohio State University, Department of Mechanical and Aerospace Engineering Wang, Yaxian; The Ohio State University, Materials Science and Engineering Rai, Akash; University of Illinois at Urbana-Champaign, Department of Materials Science and Engineering and Materials Research Laboratory Cahill, David ; University of Illinois at Urbana-Champaign, Materials Science and Engineering and Materials Research Laboratory Windl, Wolfgang; The Ohio State University, Materials Science and Engineering Heremans, Joseph; The Ohio State University, Mechanical and Aerospace Engineering; The Ohio State University, Physics; The Ohio State University, Materials Science and Engineering Goldberger, Joshua; The Ohio State University, Chemistry

SCHOLARONE™
Manuscripts

ARTICLE

Highly Efficient Transverse Thermoelectric Devices with Re_4Si_7 Crystals

Received 00th January 20xx,
Accepted 00th January 20xx

DOI: 10.1039/x0xx00000x

Michael R. Scudder,*[a] Bin He,[b] Yaxian Wang,[c] Akash Rai,[d] David G. Cahill,[d] Wolfgang Windl,[c] Joseph P. Heremans,[b,c,e] Joshua E. Goldberger[a]

The principal challenges in current thermoelectric power generation modules is the availability of stable, diffusion-resistant, lossless electrical and thermal metal-semiconductor contacts that do not degrade at the hot end nor cause reductions in device efficiency. Transverse thermoelectric devices, in which a thermal gradient in a single material induces a perpendicular voltage, promise to overcome these problems. However, the measured material transverse thermoelectric efficiencies, $z_{xy}T$, of nearly all materials to date has been far too low to confirm these advantages in an actual device. Here, we show that single crystals of Re_4Si_7, an air-stable, thermally robust, layered compound, have a transverse $z_{xy}T$ of 0.7±0.15 at 980 K, a value that is on par with existing commercial longitudinal theremoelectrics today. Through constructing and characterizing a transverse power generation module, we prove that extrinsic losses through contact resistances are minimized in this geometry, and that no electrical contacts are needed at the hot side. This excellent transverse thermoelectric performance arises from the large, oppositely signed in-plane p-type and cross-plane n-type thermopowers. These large anisotropic thermopowers arise from thermal population of the highly anisotropic valence band and isotropic conduction band in this narrow gap semiconductor. Overall, this work establishes Re_4Si_7 as the "gold-standard" of transverse thermoelectrics, allowing future exploration of unique device architectures for waste heat recovery.

Broader Context

Thermoelectric devices enable the conversion between heat and electricity, allowing active cooling or power generation from waste heat. Traditionally, these modules utilize hundreds of pairs of *p*-type and *n*-type semiconductors, with charge and heat flowing in the same "longitudinal" direction. The multitude of metal-semiconductor contacts causes large efficiency losses compared to the thermoelectric efficiency of the materials, as evaluated by their figure of merit, "*zT*". Also, the need for stable hot side metal-semiconductor contacts limits device lifetimes and operating temperatures. In "transverse" thermoelectric devices, a thermal gradient induces a perpendicular voltage, requiring only one material with one set of contacts near the cold end. Unfortunately, the transverse thermoelectric efficiencies ("$z_{xy}T$") of most materials are impractically low. Here, we show that single crystals of Re_4Si_7 have a technologically relevant $z_{xy}T$ of 0.7±0.15 at 980 K. Re_4Si_7, a layered semiconductor, simultaneously exhibits in-plane *p*-type and cross-plane *n*-type conduction. We construct a transverse thermoelectric generator from a single crystal and confirm no losses in device efficiency "$Z_{xy}T$" compared to material "$z_{xy}T$". The device contacts are moved away from the hot side, avoiding a major source of device degradation. This work establishes transverse thermoelectrics as a viable technology, and Re_4Si_7 as the "gold-standard" material.

a. Department of Chemistry and Biochemistry, The Ohio State University, Columbus, OH 43210, USA.
b. Department of Mechanical and Aerospace Engineering, The Ohio State University, Columbus, OH 43210, USA.
c. Department of Materials Science and Engineering, The Ohio State University, Columbus, OH 43210, USA.
d. Department of Materials Science and Engineering and Materials Research Laboratory, University of Illinois at Urbana-Champaign, Urbana, Illinois 61801, USA.
e. Department of Physics, The Ohio State University, Columbus, OH 43210, USA.
† Electronic Supplementary Information (ESI) available: [details of any supplementary information available should be included here]. See DOI: 10.1039/x0xx00000x

1. Introduction

The efficiency of a thermoelectric material is characterized by the dimensionless figure of merit (zT), where $zT = (\alpha^2/\rho\kappa)T$ with thermopower α, electrical resistivity ρ, and thermal conductivity κ.[1, 2] Over the past two decades, extensive research has led to the identification of *n*-type and *p*-type materials with promising zT values that are further optimized through manipulating the band structure to maximize the power factor (α^2/ρ), or via reducing lattice thermal conductivity.[2-4] This has resulted in a plethora of *p*-type and *n*-type materials with zT>1,[5] albeit in many of these emerging systems other issues including long-term thermal stability hinder their commercial viability[6] in power generation where the elements have to operate reliably at high temperatures (700-1300 K).

A conventional thermoelectric module integrates arrays of thermocouples (**Fig 1A**) made from compatible *p*-type and *n*-type thermoelectric semiconductors. Here, the elements are

connected electrically in series, and thermally in parallel. The temperature gradient and thermoelectric voltage generated occur along the same longitudinal direction. To increase this voltage in power generation or to make refrigeration modules compatible with commercially available power sources, numerous thermocouples are connected in series, resulting in the need for hundreds of metal-semiconductor contacts. Each adds an electrical contact resistance in series and a thermal contact resistance. For example, a 12 V refrigeration module made from materials with a zT between 0.9 and 1.3 give a maximum temperature drop of ΔT_M of 72 K between 280 and 350 K. It is possible to derive the device ZT to be 0.52, since $\Delta T_M=(ZT/2)T_C$, where T_C is the cold side temperature (**Supplement S1**). In essence this corresponds to a 30-50% efficiency loss over the zT of the materials.[4] In addition, in power generation applications, half of the metal-semiconductor contacts are at the hot end of the module and subject to thermal degradation. Overcoming this is one of the most challenging problems in thermoelectric power generation.[7]

Transverse thermoelectric devices in which a single material can generate a voltage perpendicular to the temperature gradient (**Fig 1B**) can circumvent these difficulties.[8, 9] Transverse devices need only two contacts that can be displaced away from the hot end, and potentially placed at the cold end of a thermoelectric generator. The device performance is now determined primarily by the geometry of a single piece of material. To increase the voltage, it is sufficient to increase its size along x; to increase its current, the size along z; and to increase the temperature drop, the size along y. The transverse thermoelectric figure of merit for a material, $z_{xy}T$, is defined[10];

$$z_{xy}T = \frac{\alpha_{xy}^2 T}{\rho_{xx}\kappa_{yy}} \quad (1)$$

Here, $\alpha_{xy} \equiv {E_x}/{\nabla_y T}$ is the transverse thermopower, the ratio of the electric field generated along x, E_x, to the temperature gradient along y, $\nabla_y T$. The thermal conductivity along y is $\kappa_{yy} \equiv {-j_{Q,y}}/{\nabla_y T}$, where j_Q is the heat flux, and $\rho_{xx} \equiv {E_x}/{j_x}$ is electrical resistivity along x, j being the current density.[8] The highest published value for $z_{xy}T$, 0.35, was reached by using the transverse thermopower created by the Nernst effect in Bi at 1 Tesla and 180 K[11] but no experimental value exceeding 0.07 was reported in the absence of a magnetic field. Contacts placed on the cold side concentrate current flow near the ends of the device (**Fig 1B**), potentially decreasing the module $Z_{xy}T$ value below the material $z_{xy}T$, but this effect vanishes asymptotically with increasing device size along x.

Anisotropic materials with different thermopower values along their crystallographic directions, (e.g. α_{IP} along the in-plane (IP) and α_{CP} along the cross-plane (CP) directions of a layered material) can have a large transverse thermopower (**Supplement S2**).[10] Cutting such a material so that the thermal gradient y is at an angle θ from the CP direction gives a non-zero transverse thermopower along x;

$$\alpha_{xy} = (\alpha_{CP} - \alpha_{IP})\sin(\theta)\cos(\theta) \quad (2)$$

The other properties ρ_{xx}, κ_{yy} and $z_{xy}T$ of the sample, expressed in the Cartesian coordinate system, can similarly be derived from the (IP, CP) values by tensor rotation[12] (**Supplement S2**). The optimal angle θ_{OPT} that maximizes $z_{xy}T$ deviates slightly from the 45° angle that maximizes α_{xy} and is material dependent.

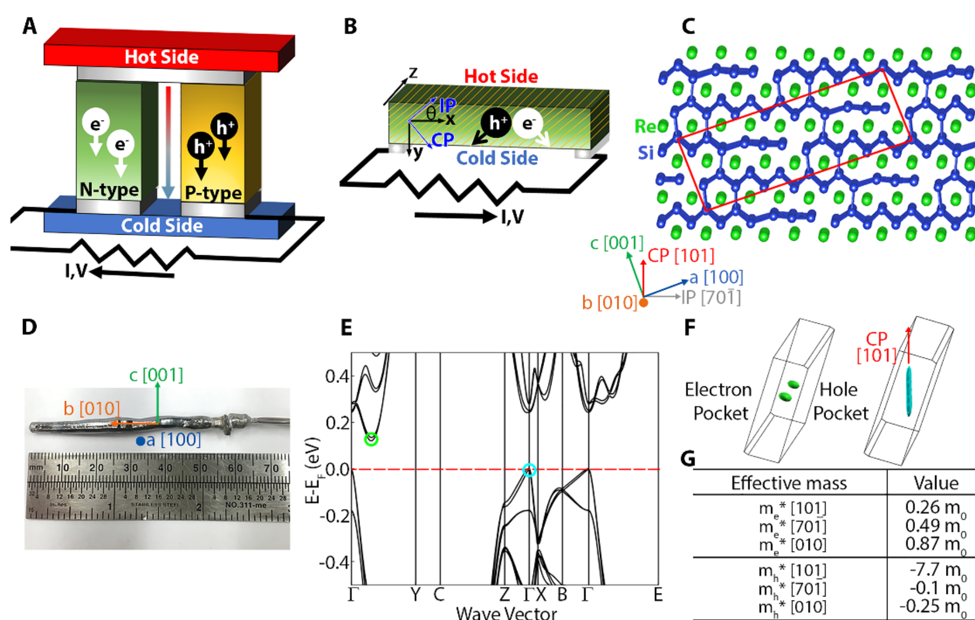

Effective mass	Value
m_e^* [101]	0.26 m_0
m_e^* [70$\bar{1}$]	0.49 m_0
m_e^* [010]	0.87 m_0
m_h^* [101]	-7.7 m_0
m_h^* [70$\bar{1}$]	-0.1 m_0
m_h^* [010]	-0.25 m_0

Fig 1 Thermoelectric devices and Re_4Si_7. **a**, Diagram of longitudinal thermoelectric device where the flow of heat and charge is colinear. Electrical and thermal contacts are made at both hot and cold ends. **b**, In a transverse thermoelectric device the heat flux (along y) is normal to the generated voltage (along x), necessitating contacts only on the cold side. Here, the in-plane (IP) and cross-plane (CP) directions of a layered material are rotated by angle (θ) away from x and y. **c**, Crystal structure of Re_4Si_7 viewed along the b axis: green, Re atoms; blue, Si atoms; Cm unit cell is highlighted in red. **d**, Single crystal with crystallographic directions indicated. **e**, Electronic band structure of Re_4Si_7. **f**, Shapes of the electron Fermi surface 0.03 eV above the conduction band minimum (**green circle in e**), and hole Fermi surface 0.015 eV below the valence band maximum (**blue circle in e**). **g**, Electron and hole effective band edge masses at the band minima, determined via DFT calculations along different directions.

This journal is © The Royal Society of Chemistry 20xx
Please do not adjust margins

From Equation (2), α_{xy} is maximized in materials where α_{IP} and α_{CP} are both large but have opposite signs. Very few materials have ever been observed to exhibit this seemingly counterintuitive behavior.[9, 13, 14] Transverse thermoelectric effects have been induced in layered composites of two different materials with highly dissimilar thermoelectric properties, including semiconductor heterostructures,[9] as well as metal/semiconductor composites.[4, 15-17] However, these materials only exhibit $z_{xy}T$ values between 0.01-0.07,[4, 12, 15, 18] which is an order of magnitude lower than conventional thermoelectric technologies.

In this work, we show that Re_4Si_7, an air-stable, thermally robust layered compound, has axis-dependent α, σ, and κ that lead to a high transverse figure of merit. Re_4Si_7 has been previously shown to simultaneously exhibit large positive and negative thermopowers along different axes.[19-24] A prior study of $ReGe_xSi_{1.75-x}$ reports thermopowers reaching α_{IP}=+150 μV K^{-1} and α_{CP}=-300 μV K^{-1},[20] yet no direct measurement of the transverse α_{xy} nor the temperature dependent thermal conductivities have been reported. Here, we start with a complete investigation of the transport properties of Re_4Si_7 along its three principal crystallographic axes (a=[100], b=[010] and c=[001]), as well as the in-plane (IP=[70$\bar{1}$]) and cross-plane (CP=[101]) directions (**Fig 1C**). The results are supported by a combination of extensive density functional theory (DFT) calculations and an analytical model that describes the physical origin of the opposite conduction polarity along different directions. We then measure the non-zero transverse thermopower α_{xy} for a sample oriented at θ_{OPT}=52° (**Supplement S2**). We show that relevant resistivities and thermal conductivities are measured to compute $z_{xy}T$, which reaches the technologically relevant level of 0.7±0.15 at 980 K.

Finally, we measure the thermodynamic efficiency of a transverse thermoelectric power generator constructed from this rotated crystal and with contacts midway between the hot and cold ends. We show that the device $Z_{xy}T$ ≈ the material $z_{xy}T$, confirming experimentally that this device geometry maximizes the performance of thermoelectric materials.

2. Results and discussion

2.1 Re_4Si_7 Thermal and Electrical Properties

Re_4Si_7 adopts a layered monoclinic crystal structure (space group *Cm*) that is a defect-ordered silicon-deficient variant of the α-$MoSi_2$ structure type with a (7a+c) × b × (c-a) supercell.[25, 26] It consists of two-dimensional layers of tetrahedrally bonded networks of Si atoms, separated by planes of Re atoms (**Fig 1C**). Furthermore, one silicon is absent for every seven Si atoms, causing a slight monoclinic distortion (β=92.8°). The a-axis and c-axis are rotated from the *IP* and *CP* directions by 22.1° and 19.3°, respectively. Multiple single crystals of Re_4Si_7 were prepared using a laser pedestal growth method in a laser diode floating zone furnace. **Fig 1D** shows a representative crystal of Re_4Si_7. Laue diffraction confirmed this crystal grew along the [010] direction and has a pseudo hexagonal cross-section with high symmetry {100} and {101} facets (**Fig S1**). The monoclinic defect-ordered structure was confirmed via Rietveld analysis of the powder X-ray diffraction data (**Fig. S1**).

Fig 1E shows the electronic band structure of Re_4Si_7. Re_4Si_7 is calculated to have an indirect band gap of 0.12 eV, consistent with previous optical absorption and reflectance measurements.[27-29] From the partial density of states, the valence band maximum primarily consists of Re 5d_{xy} orbitals which leads to a strongly

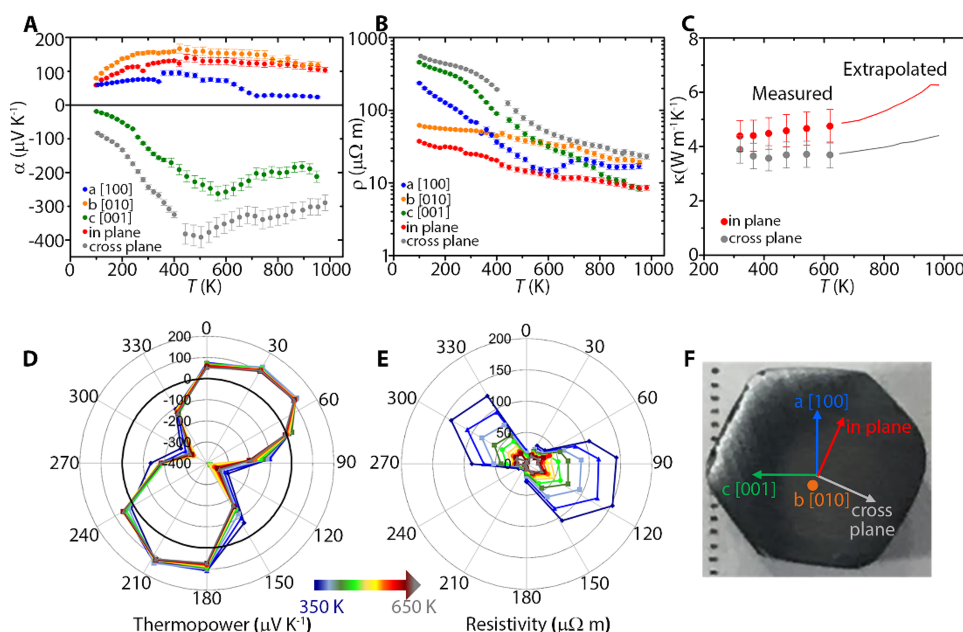

Fig 2 Thermoelectric properties for an near-intrinsic Re_4Si_7 crystal (1). **a**, Thermopower α, **b**, Electrical resistivity ρ along the principal crystallographic directions and the *IP* and *CP* direction. **c**, Total thermal conductivity (κ_{elec} + κ_{lat}) as a function of temperature. From 300-620 K, κ is measured via time domain thermal reflectance; it is extrapolated above 620 K using the Wiedemann-Franz law, assuming κ_{lat} is constant above the Debye temperature. **d**, Thermopower polar plot and **e**, electrical resistivity polar plot measured from 350-650K at different orientations along the *ac*-plane. In **d,e**, 0° corresponds to the *a* [100] **f**, Image of *ac* plane of the single-crystal with the crystallographic directions superimposed.

Please do not adjust margins

anisotropic hole pocket, while the conduction band minimum is composed of hybridized Re 5*d*-Si *3p* orbitals forming a nearly isotropic electron pocket; these features can be seen by the Fermi surfaces near the band edges (**Fig 1F**). The hole pocket has a prolate ellipsoidal shape with the long axis oriented *CP*, and the two degenerate electron pockets are nearly spherical. This causes significant differences in the effective masses and mobilities of charge carriers when they travel along different directions with respect to the atomic planes. The calculated effective masses along the *IP* and *CP* directions indicate isotropic electron mobility in all directions, while hole conduction shows low mobility (large m^*) along *CP* [101] and high mobility (small m^*) along *IP* [70$\bar{1}$] and [010] (**Fig 1G**).

We evaluated the direction dependent thermopower α, electrical resistivity ρ, and thermal conductivity κ to establish the *zT* of Re_4Si_7 (crystal 1) (**Fig 2**). The thermopower along the *a* and *b* axes, and the *IP* direction are positive across all temperatures, with 300 K values ranging from 75-155 μV K^{-1}. The same crystal has negative thermopower along the *c*-axis and the *CP* direction at all temperatures, with 300 K values of -240 and -100 μV K^{-1}, respectively. The *IP* and *CP* thermopowers approach a maximum of +160 and -386 μV K^{-1}, respectively, at 500 K. The temperature dependence of $|\alpha|$ is non-monotonic, indicating that the material is a *near-intrinsic semiconductor*. All semiconductors have a small residual non-intentional doping level, so that the chemical potential is in the conduction or valence band at very low temperatures, and $|\alpha|$ increases with *T*. With a further increase in *T*, intrinsic electrons and holes become thermally activated. When their density is sufficient to overwhelm the non-intentional carriers, the semiconductor turns intrinsic and $|\alpha|$ decreases with increasing *T* (**Supplement S3**).

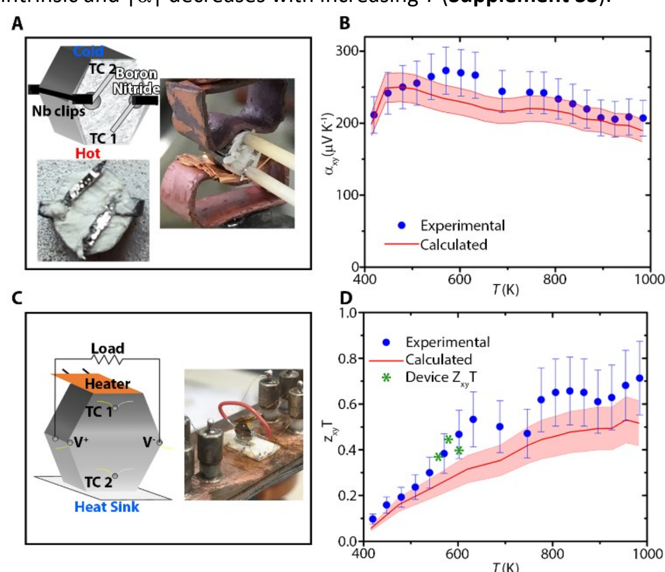

Fig 3 Transverse thermoelectric performance and ZT. **a**, Experimental setup for α_{xy} measurement; Top left: Schematic of transverse thermopower measurement setup; Bottom left: Sample prepared as outlined in schematic; Right: Sample held in place by brass fixtures. **b,** Temperature dependent α_{xy} coefficient; Measured (**closed circles**) and derived (**line**) from the measured α_{IP} and α_{CP} using equation (2). **c**, Transverse thermoelectric generator for device $Z_{xy}T$ measurement; Left: Schematic of measurement setup; Right: Device ready for measurement. **d**, Transverse thermoelectric figure of merit, $z_{xy}T$; Experimental (**closed circles**) and derived (**line**) via tensor rotations of the measured α_{IP}, α_{CP}, ρ_{IP}, and ρ_{CP}. The measured *ZxyT* values are overlaid (**green stars**).

The electrical resistivity for the same crystal from 100-980 K is shown in **Fig 2B**. Across all directions, ρ decreases with temperature, indicative of thermally activated intrinsic semiconducting behavior, and is highest along *CP* and lowest along the *IP* directions (**Fig 2E**). The angle dependent thermopowers and resistivity values were consistent across multiple repeat measurements and similar in a second crystal (crystal 2) (**Fig. S2**). The temperature dependence of total thermal conductivity is shown in **Fig 2C**. The thermal conductivity of Re_4Si_7 was measured along the *IP* and *CP* directions using the time-domain thermoreflectance method from 320 to 620 K, and extrapolated from 620 to 980 K using the Wiedemann-Franz law (**Methods**).[30] The ambipolar thermal conductivity was also estimated from the thermopower and mobility, but found to be negligible compared to the other terms as the ratio of hole to electron mobility was ~3% (**Supplement S4, Fig. S3-S5**). Angle-dependent thermopower (**Fig 2D**) and electrical resistivity (**Fig 2E**) up to 650 K are shown in polar plot form to illustrate the anisotropy of conduction behaviour within the *ac* plane of Re_4Si_7 (**Fig 2F**). The positive and negative thermopowers are maximized at the *IP* and *CP* orientations. As observed in these polar plots, the resistivity and thermopower values at a particular angle are nearly identical to those obtained upon rotating the crystal by 180°. From these measurements, Re_4Si_7 has longitudinal power factors (α^2/ρ) of 40 and 15 μW cm^{-1} K^{-2} at 900 K along the *CP* and *IP* directions, respectively, leading to longitudinal zT values of 0.8 and 0.2. These longitudinal zT values steadily increase at higher temperatures with greater population of carriers since hole transport dominates along the in-plane direction, and electron transport-along the cross-plane direction. In essence, the reduction in thermopower caused by compensation of majority carriers by increasing minority carriers at higher temperatures that typically occurs in most isotropic materials, is reduced on account of mobility difference of electrons and holes along their orthogonalized directions (**supplement S3**).

2.2 Transverse Thermoelectric Performance

Next, we evaluate the transverse thermoelectric performance of Re_4Si_7. The simultaneous *n*-type and *p*-type conduction polarities along the orthogonal directions will lead to a transverse thermopower α_{xy}, in a properly oriented crystal. When a temperature gradient is applied along the "*y*-direction" in **Fig 1B**, a voltage will be generated along the *x*-direction. This off-diagonal α_{xy} maximizes when the temperature gradient is rotated away from the *IP* and *CP* directions by an angle θ_{OPT} (**Supplement S2**). From the *IP*

This journal is © The Royal Society of Chemistry 20xx

Please do not adjust margins

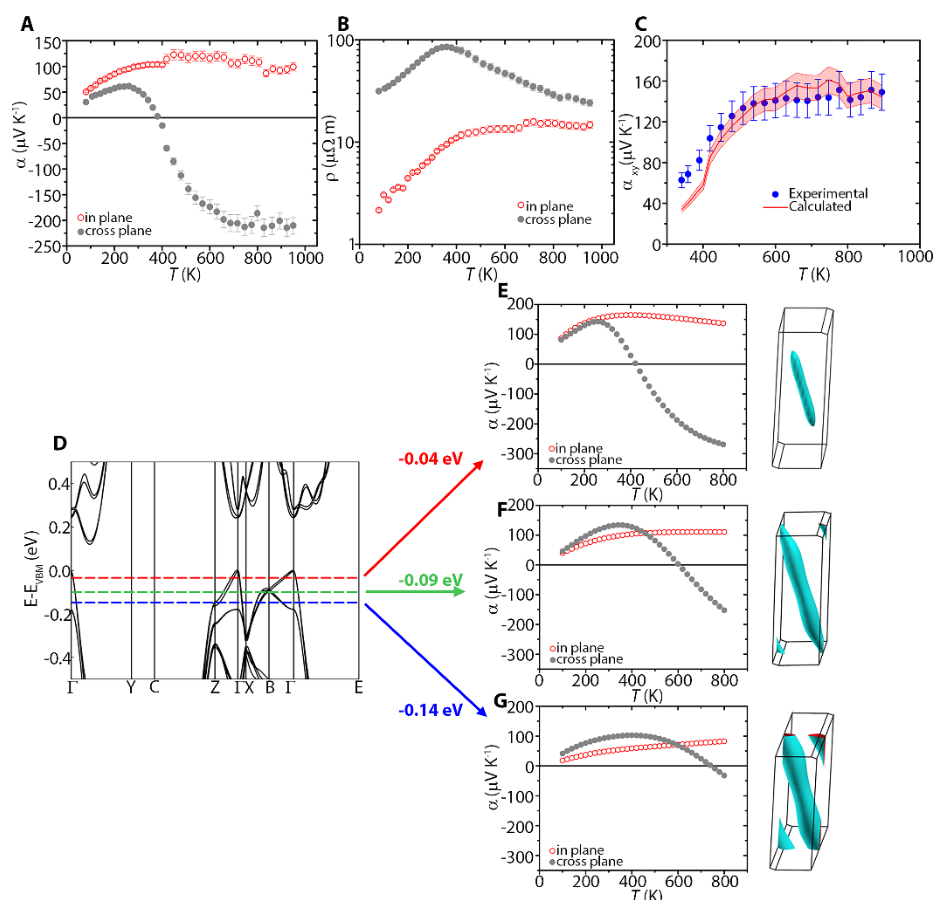

Fig 4 Anisotropic thermoelectric data for more heavily p-type Re_4Si_7 (crystal 3). *IP* and *CP* **a**, thermopowers, **b**, resistivities **c**, Transverse thermopower α_{xy} in a cut sample from 330-900 K: Experimental data and values derived from tensor rotations of α_{IP} and α_{CP}. **d,** Electronic band structure for Re_4Si_7 near the valence band maximum. **e-g)** Theoretically predicted longitudinal thermopowers (left) and Fermi surfaces (right) when doped such that **e,** E_F=40 meV, **f,** E_F=90 meV, and **g,** E_F=140 meV below the valence band maximum.

and *CP* data, an angle (θ=52°) was determined to optimize $z_{xy}T$. We developed a method to directly measure α_{xy} from 400-980 K (**Fig 3A**) which required the simultaneous measurement of the applied $\nabla_y T$ and E_x. The experimentally measured α_{xy} approached a maximum of 270±32 μV K^{-1} at 600 K, and was within error of the values derived from the measured α_{IP} and α_{CP} using equation (2) (**Fig 3B**). As a control, we confirmed a very small transverse thermopower of 15-25 μV K^{-1}, with heat flux oriented IP and electric field measured CP direction (θ=0°) (**Fig S6**). The $z_{xy}T$ at (θ_{OPT}=52°) was obtained by directly measuring ρ_{xx}, and deriving κ_{yy} via tensor rotations of κ_{IP} and κ_{CP}. At 980 K, the $z_{xy}T$ reaches 0.7±0.15 (**Fig 3D**), which is the highest transverse figure of merit reported to date. These values of α_{xy} and ρ_{xx} derived from tensor rotations of α_{IP}, α_{CP}, ρ_{IP}, and ρ_{CP}, give a $z_{xy}T$ of 0.5±0.1.

To prove that a transverse thermoelectric device suffers a considerably smaller loss in thermodynamic efficiency that a conventional thermocouple-based device, we constructed a transverse electrical generator (**Figure 3c**). A single 1.3 mm thick slab of Re_4Si_7 was cut from crystal 1, and rotated to θ=52°, and two voltage contacts were placed midway between the hot and cold ends, and mounted in a high temperature cryostat. A constantan wire load resistor impedance-matched to the sample resistance at each measurement temperature (560 K, 580 K, 600 K) was attached between the two voltage probes, and resistive heaters were placed on the hot end. At 580 K, 1 K temperature gradient was found to generate 1.5 μW of power. The thermodynamic efficiency is derived as the ratio of electrical power measured through the load over the amount of heat supplied to the sample. The latter is the amount of electrical heat minus the heat losses to the ambient. To quantify the heat losses, we repeated the measurement in the same geometry and with the same temperature difference on a quartz standard of known thermal conductivity that was cut to an identical shape as the sample (**Supplement S5**). Overall, we found that at 580 K, our transverse electric generator had a thermal efficiency equal to 9% of the Carnot efficiency. This corresponds to a device $Z_{xy}T$ of 0.44, which is nearly identical to the material $z_{xy}T$=0.42±0.08 at 580 K. The device $Z_{xy}T$ was was also nearly identical to material z_{xy}T at 560 K and 600 K, confirming consistent performance with temperature (**Fig. 3d**). This shows that a transverse device built from a single slab of single crystal Re_4Si_7 suffers only negligible device-level efficiency losses, and that contacts do not need to be placed on the hot side of the device.

2.3 Mechanism of Axis-Dependent Conduction Polarity

Axis-dependent conduction polarity in a homogeneous material has been historically attributed to the multi-carrier *p×n* mechanism[9] but can also occur via the recently discovered single-carrier goniopolar mechanism.[15] In the goniopolar mechanism, the Fermi surface must consist of a single band with a hyperboloidal shape, inducing carriers

to have either a negative or positive charge depending on the direction of travel.

In the *p×n* mechanism in intrinsic or near-intrinsic semiconductors, the electrons and holes coexist in two different bands and have strongly anisotropic carrier effective masses along different crystallographic directions. Thus, the partial contributions of electrons and holes to the thermopower strongly depends on the orientation of the crystal. As a result, this leads to a range of chemical potentials in the band gap of semiconductors where electrons dominate the thermopower along one direction and holes along another, as developed in **Supplement S6,** and **Fig S7**. We conclude that the multi-carrier mechanism is at work in near-intrinsic Re_4Si_7, consistent with previous explanations.[20] The *IP* and *CP* effective masses are highly anisotropic (nearly two orders of magnitude) at the valence band edge (**Fig 1G**), and relatively isotropic (within a factor of ~3) at the conduction band edge. The 0.12 eV gap is small enough for minority electrons to contribute considerably to the thermopower when the unintentional doping level is small.

If Re_4Si_7 was heavily *p*-type doped so that the chemical potential was -0.09 eV below the valence band, the hole Fermi surface would be hyperboloidal, implying a goniopolar mechanism (**Fig 4**). However, the experimental *IP* and *CP* thermopowers and resistivities (**Fig 4A,B**) in a more heavily *p*-type Re_4Si_7 crystal still indicate that this behavior arises via the *p×n* mechanism. Below 400 K, the CP thermopower is positive indicating that this crystal is heavily doped into the valence band. Both the *IP* and *CP* resistivities increase with temperature from 100-350 K, indicative of metallic conduction in an extrinsic semiconductor (**Fig 4B**). The slope of $\alpha(T)$ from 100-200 K, assuming acoustic phonon scattering, gives E_F ~41 mV below the valence band maximum. From the DFT simulated band structure, this corresponds to an extrinsic hole doping level of ~2×10^{19} cm^{-3}. The greater doping of this crystal leads to a smaller value of $|\alpha_{CP}|$ and thus a smaller $|\alpha_{xy}|$ in an oriented crystal (**Fig 4C**). Indeed, first principles simulations show that the temperature where α_{CP} turns negative increases as E_F is lowered further into the valence band (**Fig 4D-G**). In other words, greater thermal energy is required to sufficiently populate both the conduction and valence bands in order to achieve axis-dependent conduction polarity in heavier doped samples.

3. Conclusion

The discovery of a single thermoelectric material that can develop a transverse thermopower and $z_{xy}T$ with performance on par with existing commercial technology opens up the possibility of circumventing the most significant challenges in conventional thermoelectric generator design: the multitude of resistive, lossy high-temperature metal-semiconductor interfaces that are prone to degradation. We confirm that a Re_4Si_7 transverse thermoelectric power generator has a device thermoelectric efficiency comparable to the material $z_{xy}T$, even with contacts placed midway between the hot and cold ends. Thus, this work facilitates a "new direction" in the discovery of materials and device architectures for solid-state high-temperature electricity generation, particularly for waste heat recovery applications.

4. Experimental section

Synthesis and Characterization, Re_4Si_7

The polycrystalline Re_4Si_7 was synthesized stoichiometrically by arc-melting under Ar gas flow using high purity Re (99.99%) and Si (99.999%) powders obtained from Strem Chemicals, with a slight silicon excess. To prepare feed rods for single crystal growth, the ingots were then either re-arc melted and shaped into a 6 cm length, 5 mm diameter rod, or ground and pressed into rods via cold isostatic pressing (AIP3-12-60C Research CIP). The phase purity of the samples was verified by X-ray diffraction, using Cu Kα1 radiation (Bruker D8). Single crystals of ~4 cm in length were grown from feed rods at a growth rate of ~5 mm/hr under an Ar gas flow using a modified laser pedestal growth technique in a Laser Diode Floating Zone furnace, and this gave crystals 1 and 2. The more heavily doped crystal 3 came from feed rods prepared by cold isostatic pressing, which had a much larger diameter and required higher laser powers to achieve a molten zone. This led to greater Si volatilization during growth. We attribute *p*-type doping to arise from Si vacancies (**Supplement S7, Fig. S8**). The crystallographic orientations of the as-grown single crystals were verified by Laue diffraction and were then diced along [100] for transport measurement.

Thermopower and Electrical Measurements

Low temperature transport properties were measured in a modified Janis cryostat system. In the cryostat, the transport properties were measured from 80 to 400 K, with a magnetic field from -1.4 to 1.4 T, using a set-up that has been described previously.[14] For cryostat measurements along each respective axis, a heater is attached perpendicular to the crystallographic direction so that the temperature gradient is applied along that direction of interest. A copper heat spreader under the resistive heating element atop the sample and a hexagonal boron nitride heat sink below the sample assured uniform heat flow in the samples. Two copper-Constantan thermocouples are attached to the top and bottom of the sample below the heater to measure the voltage and temperature gradient. Current wires are placed at the top and bottom of the sample for electrical resistance measurements. Two different 5 mm slabs of single-crystalline Re_4Si_7 were measured in the low temperature-range cryostat system, with consistent results.

High temperature transport properties were measured in a Linseis LSR-3. Thermopower and electrical resistivity were simultaneously measured from 330 to 950 K at zero magnetic field. LSR measurements were performed under a positive pressure inert gas (helium) environment. A homebuilt brass sample holder was used as a heat spreader and to keep the Re_4Si_7 single crystal sample at a fixed position during each measurement. Small strips of palladium foil (<1 mm thickness) were used to separate the thermocouple probes (Type S) from the sample to avoid contamination at high temperatures. Two different 5 mm slabs of single-crystalline Re_4Si_7 were measured in the high temperature-range Linseis, with consistent results. When the crystal was flipped to contact the back face back face The thermopower and resistivity particular orientation was within error.

 This journal is © The Royal Society of Chemistry 20xx

Please do not adjust margins

Thermal Conductivity Measurements

The thermal conductivity of Re_4Si_7 was measured along the IP and CP crystallographic orientations using the time-domain thermoreflectance method. The single-crystalline sample was measured from 320 to 620 K using an aluminum thin film transducer on the sample surface. The thermal conductivity was measured upon both heating and cooling cycles to confirm precision of data. The temperature-dependent heat capacity of WSi_2 was used for the measurement due to its similar Dulong-Petit values as Re_4Si_7. At 620 K, the lattice and electronic contributions, κ_{lat} and κ_{elec} were estimated: κ_{elec} was derived from ρ using the Wiedemann-Franz (WF) law, and κ_{lat} derived as κ - κ_{elec}. Above 620 K, κ along the IP and CP directions was extrapolated again deriving $\kappa_{elec}(T)$ from $\rho(T)$ using WF, and assuming that κ_{lat} was constant, κ_{lat} (T > 620 K) = κ_{lat} (620 K). An experimental measurement of κ using TDTR was not possible above 620 K, as a suitable transducer material that did not lead to surface degradation of the sample could not be identified. The free-electron value for the Lorenz ratio of 2.44×10^{-8} W Ω K^{-2} was used for this extrapolation.

Transverse Thermopower Measurements

The transverse thermopower α_{xy} was measured in the Linseis LSR-3 from 330 to 1000 K. A home built brass sample holder was again used to keep the single crystal at a fixed rotation during each measurement. To avoid detecting thermopower signals related to a longitudinal thermopower α_{xx} or α_{yy}, a boron nitride spray coating was applied to the faces of the sample to provide electrical insulation but maintain thermal contact between the sample and the spring-loaded thermocouple electrodes in order to directly measure heat gradient **(Fig 3A)**. To measure transverse thermopower, rigid niobium clips were affixed to the sample to tightly pin down thin strips of palladium that gave direct electrical contact from points on each side of the sample (transverse direction) and the thermocouple probes (longitudinal direction). As a result, α_{xy} could be directly measured in this setup. The measured α_{xy} was normalized by a geometrical factor taking into consideration distance between longitudinal thermocouple probes (ΔT length) and transverse voltage probes (ΔV length). Immediately following this measurement, the crystal was rotated an additional 90 degrees to measure the corresponding ρ_{xx}. The rotation of the crystal was confirmed using image analysis software. The values and method was confirmed on multiple 5 mm long diced sections along the length of the single crystal and compared to experimental prediction within error.

To experimentally predict transverse thermopower coefficients prior to direct measurement, the longitudinal thermopower and electrical resistivity for the in-plane and cross-plane orientations were measured on the Linseis. Once these data were collected, α_{xy} was predicted from tensor rotations described in the extended discussion (**Supplement S2**). These predicted data were treated with error propagation described below.

Computational Details

The density functional theory (DFT) calculations were performed using the Vienna *ab initio* Simulation Package (VASP)[31] with projector-augmented wave (PAW) potentials based on the Perdew Burke Ernzerhof (PBE) exchange-correlation functional.[30, 32] A 4×18×6 Γ-centered k-mesh[33] and a plane-wave cut-off of 320 eV were employed for the calculations. The lattice parameters of a = 23.164 Å, b = 3.147 Å, c = 8.288 Å, and β = 92.77° and atomic positions from Ref.[25] were used for all calculations of the perfect structure, and the structure was only relaxed for the vacancy calculations in **Supplement S8**. Additionally, spin orbit coupling (SOC) effect was taken into account. Since electron correlations in the Re *d*-orbitals have a strong influence on the electronic structure of Re_4Si_7, a Hubbard-U of 2 eV was used for the Re *d*-orbitals within the rotationally invariant Dudarev approach[34] which produces a band gap that matches the experimental value of 0.12 eV.

Experimental Error Bars

For longitudinal thermopower measurements done in the cryostat (low temperature region), the error of thermopower and resistivity was determined to be 3%. This was calculated based on the value of $\Delta L_T/L_T$, or the diameter of silver epoxy used to affix copper (voltage) wires to the sample divided by the length between the wires. Care was taken to use as little silver epoxy paste as possible to minimize heat dissipation from the sample through the electrical contacts. Sample cross-sectional areas were measured both manually with calipers and digitally with image processing software to confirm the dimensions.

The thermal conductivity of Re_4Si_7 and the Al interface conductance at each temperature was taken as the average of the measured values in each heating and cooling cycle. The statistical error was calculated as twice the standard deviation of the measured values from the mean value. The volumetric heat capacity of Re_4Si_7 was used as a fixed parameter in our thermal diffusive model. Since we could not find any experimental or theoretical values for the temperature-dependent volumetric heat capacity of Re_4Si_7 at elevated temperatures, the values for WSi_2 that have been directly measured up to 1200 K were used.[35] Confirming that WSi_2 and Re_4Si_7 will have similar specific heats, low temperature (2-300 K) heat capacity measurements on Re_4Si_7 were performed and indicated a Dulong-Petit value of 3.029 J cm^{-3} K^{-1} which is within 0.3% of WSi_2 (3.021 cm^{-3} K^{-1}).[35] In addition, analysis of data acquired in time domain thermoreflectance experiments requires accurate measurements of the Al film optical transducer thickness. The transducer absorbs energy from the pump optical pulse and provides a temperature-dependent reflectivity that is interrogated by the probe optical pulse. This thickness measurement was accomplished using picosecond acoustics, which yield an echo time is determined to have an error of 4%, resulting in a 4% error of measured Al film thickness. The total error of thermal conductivity is set to 13%, as this accounts for both the error in the volumetric heat capacity data used as well as the error in Al thin film transducer thickness.

This journal is © The Royal Society of Chemistry 20xx

Please do not adjust margins

For longitudinal thermopower and electrical resistivity measurements in the Linseis LSR-3 (high temperature region), the error of both thermopower and resistivity was calculated to be 8%. This higher error relative to cryostat measurements is a result of the larger thermocouple probe tip diameter in the Linseis instrument.

For transverse thermopower measurements (α_{xy}) in the Linseis, the error in measured longitudinal temperature gradient as well as the error in measured transverse thermopower have an additive effect and thus were both taken into consideration. The ratio of thermocouple tip diameter to distance between thermocouples, ($\Delta L_T/L_T$), represented the error in longitudinal temperature gradient. The ratio of electrical contact diameter to transverse distance between electrical contacts, ($\Delta L_E/L_E$), represented the error in measured transverse thermopower. As a result, the total error in measured transverse thermopower from these sources was 12%.

To determine the error in experimental transverse $z_{xy}T$, the square of the sums of the errors for transverse thermopower (α_{xy}), electrical resistivity (ρ_{xx}), and thermal conductivity (κ_{yy}) in the temperature range of interest was determined, and this value was 23%.

To determine the error in derived transverse $z_{xy}T$, the square of the sums of the errors for longitudinal thermopower (α_{xx}), electrical resistivity (ρ_{xx}), and thermal conductivity (κ_{yy}) was determined, and this value was 19%. The error for longitudinal thermopower, resistivity, and thermal conductivity, was used as the error for the α_{xy}, ρ_{xx}, and κ_{yy} values derived from the tensor rotations of the measured in-plane and cross-plane longitudinal thermopower.

Conflicts of interest

There are no conflicts to declare.

Acknowledgements

Primary funding this work synthesis, theory, and transport measurements (M.R.S., J.E.G., Y.W., and W.W.) was provided by AFOSR project no. FA9550-18-1-0335 and DOE grant number DE-SC0020923 (J.P.H.). Funding for thermal conductivity measurements (A.R., D.G.C.) and transport measurements (B.H. and J.P.H.) was provided by NSF EFRI-1433467. This material is based upon single crystal growth supported by the: National Science Foundation (Platform for the Accelerated Realization, Analysis, and Discovery of Interface Materials (PARADIM)) under Cooperative Agreement No. DMR-1539918. Computations were performed on the machines of the Ohio Supercomputer Center under project no. PAS0072.

Author Contributions

Single crystal growth was performed by M.R.S. and J.E.G at PARADIM. Electronic Transport measurements were conducted by M.R.S., B.H., J.E.G., and J.P.H. Thermal Conductivity Measurements were conducted by A.R. and D.G.C. Computations were performed by Y.W. and W.W. The manuscript was written primarily by M.R.S., J.E.G., and J.P.H. with contributions by all authors.

References

1. J. P. Heremans, M. S. Dresselhaus, L. E. Bell and D. T. Morelli, *Nat. Nanotechnol.*, 2013, **8**, 471-473.
2. J. He and T. M. Tritt, *Science*, 2017, **357**, 1-9.
3. K. Biswas, J. He, I. D. Blum, C. I. Wu, T. P. Hogan, D. N. Seidman, V. P. Dravid and M. G. Kanatzidis, *Nature*, 2012, **489**, 414-418.
4. T. Kanno, A. Sakai, K. Takahashi, A. Omote, H. Adachi and Y. Yamada, *Appl. Phys. Lett.*, 2012, **101**, 3-6.
5. G. Tan, L.-D. Zhao and M. G. Kanatzidis, *Chem. Rev.*, 2016, **116**, 12123-12149.
6. X. F. Zheng, C. X. Liu, Y. Y. Yan and Q. Wang, *Renewable Sustainable Energy Rev.*, 2014, **32**, 486-503.
7. M. Hamid Elsheikh, D. A. Shnawah, M. F. M. Sabri, S. B. M. Said, M. Haji Hassan, M. B. Ali Bashir and M. Mohamad, *Renewable Sustainable Energy Rev.*, 2014, **30**, 337-355.
8. H. J. Goldsmid, *J. Electron. Mater.*, 2011, **40**, 1254-1259.
9. Y. Tang, B. Cui, C. Zhou and M. Grayson, *J. Electron. Mater.*, 2015, **44**, 227701.
10. H. J. Goldsmith, *Introduction to Thermoelectricity*, Springer, Berlin, 2010.
11. P. Jandl and U. Birkholz, *J. Appl. Phys.*, 1994, **76**, 7351-7366.
12. C. Zhou, S. Birner, Y. Tang, K. Heinselman and M. Grayson, *Phys. Rev. Lett.*, 2013, **110**, 227701.
13. Y. Wang, K. G. Koster, A. M. Ochs, M. R. Scudder, J. P. Heremans, W. Windl and J. E. Goldberger, *J. Am. Chem. Soc.*, 2020, **142**, 2812-2822.
14. B. He, Y. Wang, M. Q. Arguilla, N. D. Cultrara, M. R. Scudder, J. E. Goldberger, W. Windl and J. P. Heremans, *Nat. Mater.*, 2019, **18**, 568-572.
15. T. Kanno, S. Yotsuhashi, A. Sakai, K. Takahashi and H. Adachi, *Appl. Phys. Lett.*, 2009, **94**, 1-3.
16. C. Reitmaier, F. Walther and H. Lengfellner, *Appl. Phys. A.*, 2010, **99**, 717-722.
17. C. Reitmaier, F. Walther and H. Lengfellner, *Appl. Phys. A.*, 2011, **105**, 347-349.
18. K. Takahashi, T. Kanno, A. Sakai, H. Tamaki, H. Kusada and Y. Yamada, *Sci. Rep.*, 2013, **3**, 1-3.
19. A. B. Filonov, A. E. Krivosheev, L. I. Ivanenko, G. Behr, J. Schumann, D. Souptel and V. E. Borisenko, *Semiconductors*, 2005, **39**, 395-399.
20. J. J. Gu, M. W. Oh, H. Inui and D. Zhang, *Phys. Rev. B: Condens. Matter Mater. Phys.*, 2005, **71**, 4-7.
21. M.-W. Oh, J.-J. Gu, H. Inui, M.-H. Oh and D.-M. Wee, *Phys. B*, 2007, **389**, 367-371.
22. A. Qiu, L. Zhang, A. Shan and J. Wu, *Phys. Rev. B*, 2008, **77**, 1-6.
23. F. Wang, I. Veremchuk and S. Lidin, *Eur. J. Inorg. Chem.*, 2017, **2017**, 47-55.
24. S. Harada, K. Tanaka, K. Kishida and H. Inui, *Advanced Materials Research*, 2007, **26-28**, 197-200.
25. D. C. Fredrickson, M. Boström, Y. Grin and S. Lidin, *Chem. - Eur. J.*, 2009, **15**, 8108-8112.
26. S. Harada, H. Hoshikawa, K. Kuwabara, K. Tanaka, E. Okunishi and H. Inui, *Philos. Mag.*, 2011, **91**, 3108-3127.

This journal is © The Royal Society of Chemistry 20xx

Please do not adjust margins

27. R. G. Long, M. C. Bost and J. E. Mahan, *Thin Solid Films*, 1988, **162**, 29-40.
28. T. Siegrist, F. Hulliger and G. Travaglini, *J. Less-Common Met.*, 1983, **92**, 119-129.
29. I. Ali, P. Muret and T. A. Nguyen Tan, *Appl. Surf. Sci.*, 1996, **102**, 147-150.
30. D. G. Cahill, *Rev. Sci. Instrum.*, 2004, **75**, 5119-5122.
31. G. Kresse and J. Hafner, *Phys. Rev. B*, 1993, **47**, 558-561.
32. J. P. Perdew, K. Burke and M. Ernzerhof, *Phys. Rev. Lett.*, 1996, **77**, 3865-3868.
33. H. J. Monkhorst and J. D. Pack, *Phys. Rev. B*, 1976, **13**, 5188-5192.
34. S. L. Dudarev, G. A. Botton, S. Y. Savrasov, C. J. Humphreys and A. P. Sutton, *Phys. Rev. B*, 1998, **57**, 1505-1509.
35. Y. S. Touloukian, *Specific Heat: Nonmetallic Solids*, Plenum, New York, 1970.

This journal is © The Royal Society of Chemistry 20xx